ABSTRACT

Title of Thesis:	TOWARDS THE SYNTHESIS OF PNAG CROSSLINKERS TO IDENTIFY PROTEIN BINDING PARTERNS
	Kevin Richard Mrugalski, Masters of Science, Chemistry
Thesis Directed By:	Dr. Myles Poulin, Department of Chemistry and Biochemistry

Bacterial biofilms are of concern in medicine due to natural drug resistance. Many bacterial species that infect humans including *Escherichia coli, Staphylococcus aureus, Pseudomonas aeruginosa,* and *Vibrio cholera* form. Poly β-(1→6)-*N*-acetyl-D-glucosamine (PNAG) is a major component of biofilms and has been found to play a key role in the early stages of the biofilm life-cycle. However, little information is known about what proteins interact with this important polysaccharide. Our goal is to create small PNAG analogues to covalently capture and identify PNAG binding partners in *E. coli,* an important model organism. PNAG analogues will contain photoaffinity groups, that when activated, covalently link associated proteins to the probe. Using a proteomics-mass spectrometry-based approach, PNAG binding partners will be identified. We describe the efforts and challenges encountered

synthesizing the final PNAG probes. New synthetic routes are proposed based on literature precedent that will enable synthesis of the desired compounds.

TOWARDS THE SYNTHESIS OF PNAG CROSSLINKERS TO IDENTIFY PROTEIN BINDING PARTNERS

by

Kevin Richard Mrugalski

Thesis submitted to the Faculty of the Graduate School of the
University of Maryland, College Park, in partial fulfillment
of the requirements for the degree of
Masters of Science,
Chemistry
2019

Advisory Committee:
Professor Dr. Myles Poulin, Chair
Dr. Philip DeShong
Dr. Osvaldo Gutierrez
Dr. Lai-Xi Wang

Table of Contents

List of Figures

List of Schemes

Introduction:

Bacterial biofilms consist of communities of bacteria that are attached to a surface[1], and pose a major concern in the medical industry. There is an increasing prevalence of antibiotic-resistant infections, including those by methicillin resistant *Staphylococcus aureus* (MRSA), which result from highly virulent biofilm-forming bacterial strains[2,3]. Other bacteria also form biofilms, including *Escherichia coli*, *Pseudomonas aeruginosa*, and *Vibrio cholera*, and the formation of biofilm contributes to their associated diseases (urinary tract infection, cystic fibrosis complications, and cholera, respectively).[3,4] Despite the problems caused by biofilms in our society, the factors that regulate their formation are not well understood. Understanding how biofilms grow and mature could lead to the discovery of new treatments to combat their inherent drug resistance, or to modulate biofilm formation to better serve our purposes.

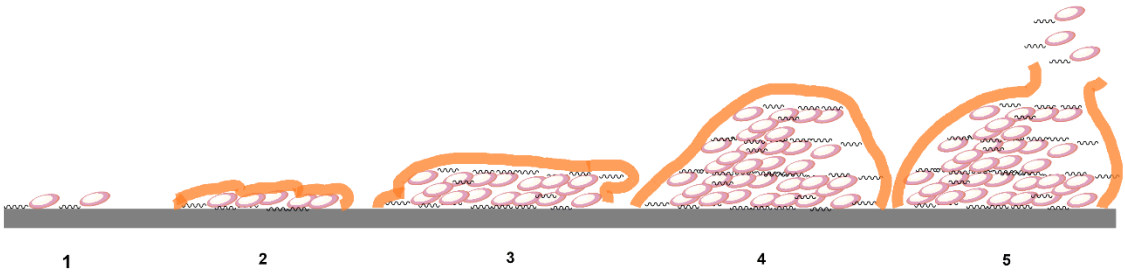

Figure 1: Life cycle of biofilms. (1) Initial cell attachment; (2) cell division and EPS secretion, irreversible attachment, (3) multi-layered cell clusters, early biofilm stage, (4) mature biofilm, (5) planktonic cell release and colonization.[5]

The biofilm life-cycle has five stages beginning with planktonic bacterial cells. First, a single planktonic bacterium attaches itself transiently to a surface (**Figure 1-1**).[5] The bacterium begins dividing and reproduces forming a small colony

on the surface accompanied by a transition to permanent surface attachment (**Figure 1-2**), which is key for further biofilm development for most bacteria.[5] Also, at this stage, the bacteria begin to secrete an extracellular polymeric substance (EPS) (**Figure 2**) composed of extracellular DNA (eDNA), proteins, lipids, and exo-polysaccharides.[6] The colony is classified as a biofilm at the third stage (**Figure 1-3**), and is characterized by multi-layered cell clusters.[5] The fourth stage involves biofilm maturation to form complex three dimensional cell networks imbedded within the EPS and offers the best protection against antibiotics (**Figure 1-4**).[5] The final stage involves the release of planktonic bacterial cells from the mature biofilm to colonize a new surface (**Figure 1-5**).[5] While the general steps of the biofilm life-cycle are well established, there is still relatively little known about the specific interactions in the EPS that regulate each step of biofilm formation and structure.

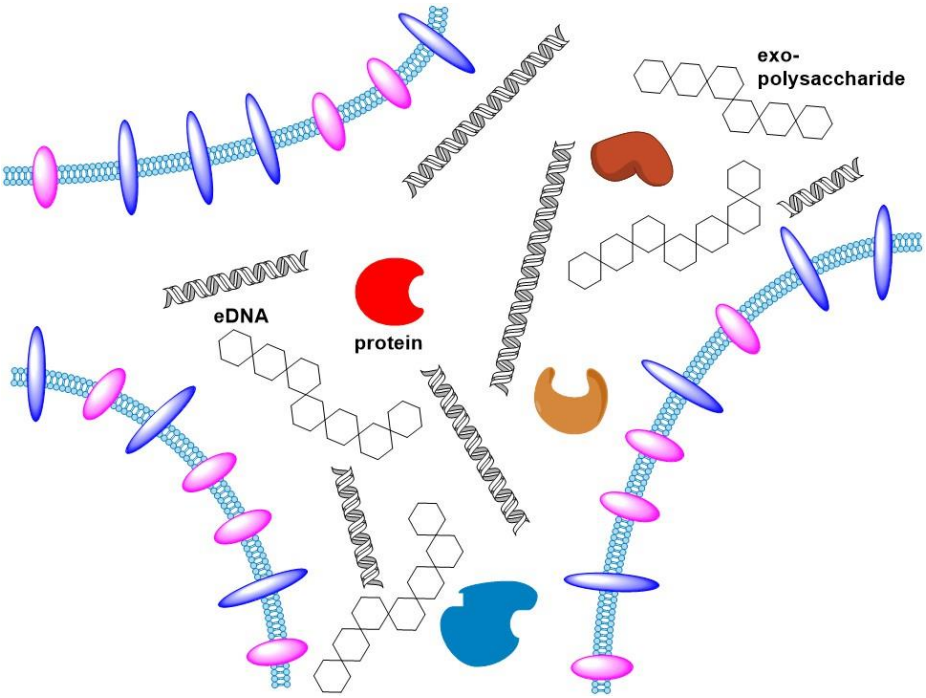

Figure 2: The major components of the EPS are extracellular DNA (eDNA), proteins, and exo-polysaccharides.

Understanding the structure and function of the EPS is a target of current research due to its secretion in the early stages of biofilm formation and as a result of its critical functions supporting biofilms. These include providing mechanical structure to the biofilm, aiding in metabolism, and protecting cells from the outside environment. [3,4,6] The EPS aids to anchor cells of the biofilm to a surface mainly through exopolysaccharide secretion and eDNA, depending on the species.[6,7] Additionally, the EPS contributes to the often highly ordered structure of the biofilm, by facilitating cell–cell attachment and increasing cell density, which gives the biofilm stability.[6,8,9,10,11,12] The EPS aids in cellular metabolism by sequestering enzymes that digest outside components as well as the EPS itself, including exo-polysaccharides, which is important to release planktonic bacteria in the later stages of the biofilm life cycle. [1,6,13] The EPS is responsible for protecting the biofilm from the outside environment through a variety of mechanisms. First, the EPS also retains water, which is essential to keep the biofilms hydrated in dry environments.[6] Also, the eDNA present in the EPS is used to transfer genetic information between bacteria, conferring greater antibiotic resistance to the biofilm as a whole.[6] Lastly, the EPS acts as a physical barrier between the biofilm and the outside environment analogous to skin.[6] The exo-polysaccharide component of the EPS is known to slow diffusion of antibiotics and harmful toxins.[6,3]

Exo-polysaccharide components of the biofilm EPS play an important role in maintaining biofilm structure and cell-surface attachment, which are key factors in biofilm growth and development. For example, in *V. cholera*, vibrio polysaccharide (VPS) the critical exo-polysaccharide in *V. cholera* has been shown to bind the

protein RmbA to facilitate proper cell–cell attachment and maintain the proper architecture of the biofilm.[8,14] Mutants lacking RmbA produced biofilms that are larger but more susceptible to mechanical disruption due to the lack of cell–cell connections.[14] The RmbA–VPS interaction is one of the first protein/exo-polysaccharide interaction to be observed and suggest an important role of exo-polysaccharides in maintain cell–cell contact through protein–carbohydrate binding interaction during biofilm development.

In addition to VPS, the exo-polysaccharide, poly β-1,6-*N*-acetyl-D-glucoseamine (PNAG) (**Figure 3)** is an important adhesion factor in several bacterial species and was first discovered first in *S. epidermidis* in 1999.[15] Since the discovery of PNAG, there have been key studies over the past 20 years that further support its importance in other species of bacteria. For example, in 2005, PNAG was discovered to be important for the organization of *E. coli* strain K12 cells.[16] This was done by creating a mutant that lacked the necessary glycotransferase PgaC, which is responsible for PNAG export, and determining the difference in attachment patters compared to the wild type.[16] Mutant and wild type cells were allowed to grow on a slide for 4 hours, then the slide was inverted and the number of cells on the slide were counted at 10 min intervals for 1 hour.[16] Additionally, fast Fourier transform spectra were taken at the start of the growth assay and at 20 min and 60 min.[16] Based upon fast Fourier transform analysis, ΔpgaC mutants showed no defined structure after 60 min, as compared to the wild-type.[16] The further disorganization of the ΔpgaC mutants cells was confirmed by microscopy, as the cells were mainly attached to the surface at the poles and were not observed to form the proper cell–cell connections.[16]

The lack of cell–cell connections was seen by the gravity displacement assay described above as the cell density of the ΔpgaC mutant decreased over the course of 60 min and the cells were not able to form a 3-D biofilm.[16] These observations indicated that PNAG may be an important adhesion factor for the K12 strain as well as an important factor in maintaining the structure of the cells during biofilm maturation.[16]

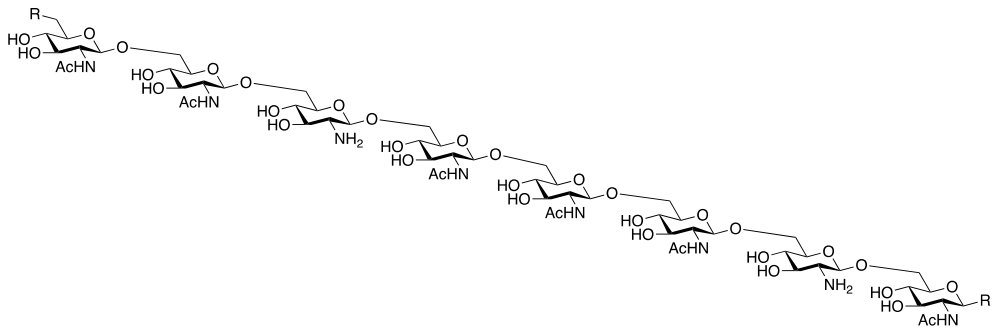

Figure 3: General structure of PNAG. On average, 10-20% of residues are deacetylated.

In addition to *E. coli*, PNAG is also found in other human pathogens and is an important adhesion factor in gram-negative bacteria such as *V. cholera*[14] and *Acinetobacter baumanii*[17], as well as gram-positive bacteria *S. aureus*[18] and *Staphylococcus epidermidis*[19], which commonly infect medical devices. For all of these species, biofilm is a major virulence factor in animal infection models[20] and blocking cell-EPS interactions is a potential strategy for the development of drugs to inhibit biofilm development. Recently, progress has been made in understanding the proteins that control PNAG synthesis and export. In 2018, a study was published describing how the manipulation of PNAG synthesis and transportation proteins can disrupt biofilm formation.[21] In this study, the authors mutated the protein PgaB which

is encoded by the *pgaABCD* operon along with other proteins that control PNAG synthesis and export in *E. coli*.[22] PgaB is a two-domain periplasmic protein which contains a *N*-terminal carbohydrate esterase domain as well as a *C*-terminal PNAG binding domain which facilitates PNAG export from the cell.[21] The *C*-terminal domains for both *E. coli* and *Bordetella bronchiseptica* were able to hydrolyze deacetylated PNAG (dPNAG) from *S. aureus*, and were shown to disrupt PNAG dependent biofilms of *Bordetella pertussis, Staphylococcus carnosus, S. epidermidis,* and *E. coli*.[21] Additionally, it was determined that the PgaB domains of both species hydrolyzed dPNAG with a GlcN-GlcNAc-GlcNAc motif at the reducing end of the new fragment, indicating that the deacetylation state of PNAG is important for cleavage and export.[21] Overall, this work indicates strongly that PNAG is an integral part of the biofilm, as the hydrolysis of PNAG by the C-terminal domain of *B. bronchiseptica* and *E. coli* PgaB was able to disrupt biofilms that utilize PNAG in multiple species.

Research Plan:

It is clear that PNAG plays a critical role in the structure and development of bacterial biofilms, but exactly how it contributes to biofilm development at a molecular level remains elusive. To that end, ***the goal of this project is to identify and characterize PNAG binding protiens using a targeted proteomics approach. This will lead to a better understanding of the mechanisms by which PNAG functions in biofilm growth and development in E. coli, an important model organism.*** Protein–carbohydrate binding interactions are frequently hard to capture and characterize as the interactions are frequently transient and have low affinity (K_d

of μM to mM).[23] Therefore, to capture these low affinity binding interactions we plan to use a photoaffinity-labeling based strategy to covalently cross-link the PNAG probe to the target protein, allowing for analysis of the protein using mass-spectrometry based approaches.[24,25] For our approach, a diazirine functional group was selected as the photoactivatable cross-linking group for several reasons. Diazirines are a photo-active protein crosslinking functional group that forms a highly reactive carbene when exposed to UV light around 365 nm (**Figure 4**). This carbene then can insert itself into O-H, C-H, S-H, and N-H bonds of proteins that are in close proximity to the carbene, forming a permanent covalent linkage. Since the diazirine is indiscriminate in terms of where it inserts, we should be able to capture most protein-PNAG associations with this probe. Another benefit to using diazirines over other photoactive groups, such as aryl azides and benzophenones, is that diazirines are more reactive and less bulky, and are therefore less likely to interfere with normal binding interactions between the probe and target proteins.

Figure 4: Mechanism of diazirine degradation and insertion into O-H, C-H, S-H, or N-H bonds.

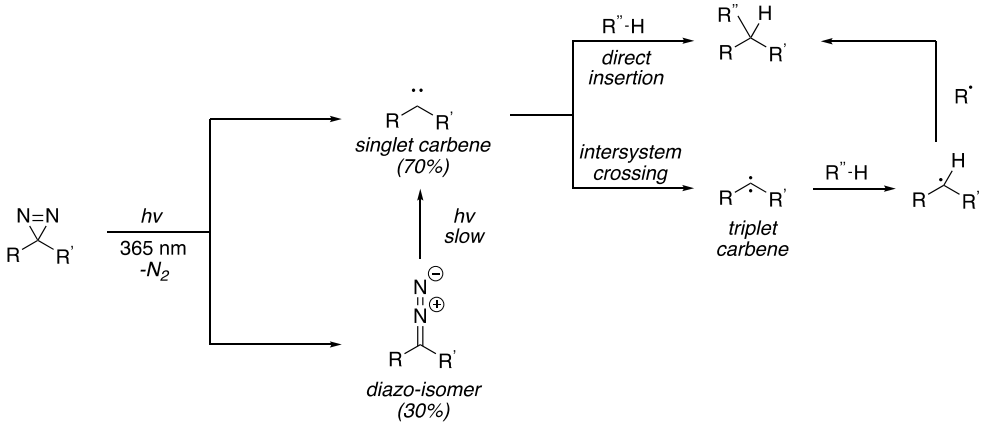

We will incorporate the diazirine onto short segments of synthetic PNAG around 6–10 monosaccharide units in length (**Scheme 1**). We took inspiration from a

paper published in 2009 by Nitz and coworkers that described a synthesis of PNAG probes using HF·pyridine to synthesize short polymers of *N*-acetyl-D-glucosamine to the desired length of our probes.[26] After the initial PNAG probe is constructed, we will attach the diazirine moiety to our PNAG using two different methods (**Scheme 1**).

We chose to explore two different methods to link a diazirine reactive group to our PNAG oligosacharides (**Scheme 1**). First, in the type I probe the diazirine, which is derived from levulinic acid using literature methods[27,28], is attached to a free primary amine of GlcN residues present in the PNAG as the NHS ester (compound **4**). A potential downside of this approach is that the diazirine will be incorporated at variable positions along the PNAG polymer chain, leading to a heterogeneous mixture, which may affect protein binding and capture. Additionally, the modified levulinc acid could interfere with protein active sites and important PNAG-protein interactions may not be captured effectively. As an alternative, the type II probe incorporates the diazirine on a bifunctional linker (compound **5**) via the anomeric position, eliminating the variability.[26,29] The main difficulties with this strategy are the complex route to the synthesis of compound **5** and the coupling of compound **5** with the anomeric position of compound **3**.

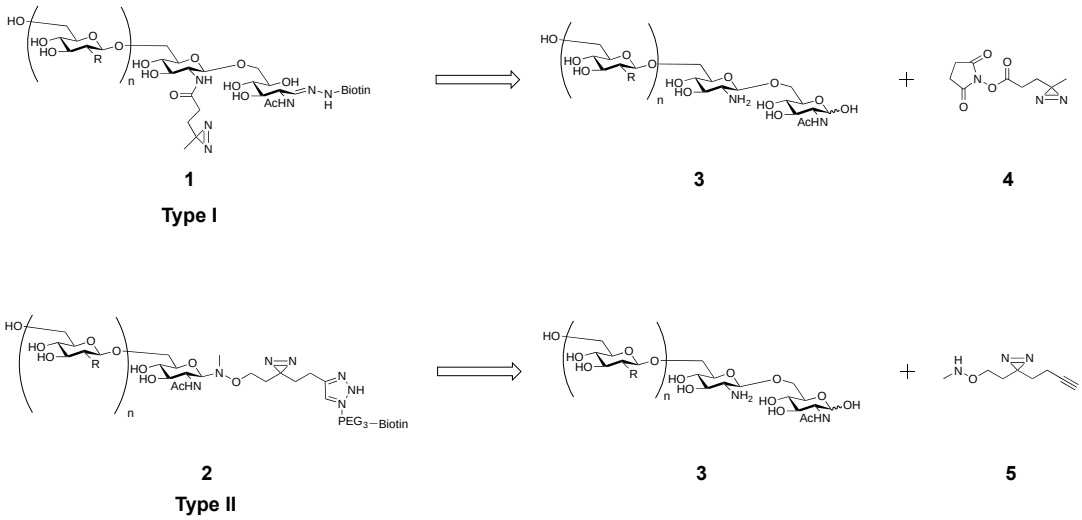

Scheme 1: Type I and Type II probes that will be used to conduct binding experiments with *E. coli* cell lysate. Each probe type incorporates the diazirine at different positions in the PNAG backbone.

Once both probes are synthesized, we then plan incubate the probes with cell lysate derived from cultures of *E. coli* biofilms (**Figure 5**). Then, we will activate the diazirine with UV light, which will cross-link the PNAG probe to any interacting proteins. The probe and cross-linked proteins will be isolated and enriched through streptavidin affinity purification using streptavidin coated magnetic beads and washed to eliminate any proteins that are not covalently cross-linked. Proteins attached to the probe will be digested with trypsin and the free amines on the peptide will be methylated using sodium cyanoborohydride and formaldehyde and versions with heavier isotopes to generate a mass difference between the peptides from PNAG and

the two controls.[30] From there, we can see if any characterized proteins interact with PNAG and potentially study these proteins in the future.

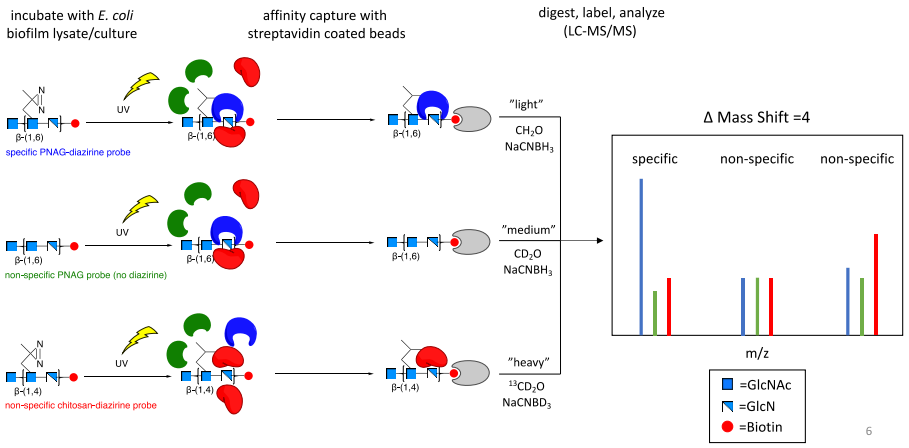

Figure 5: Approach to isolate and characterize PNAG binding partners using a targeted-proteomics approach. A PNAG probe without the photoaffinity ligand and a chitosan probe including the photoaffinity ligand will act as negative controls.

A common problem associated with targeted-proteomics based approaches is differentiating between non-specific and specific binding interactions captured with the affinity probes. Our approach will incorporate two controls to account for non-specific interactions: one using a synthetic PNAG probe lacking the diazirine moiety and the other employing chitosan as the backbone for the probe (**Figure 5**). Chitosan is composed of glucosamine linked through β-(1→4) glycosidic bonds instead of the β-(1→6) linkages found in PNAG. This difference in the glyosidic linkage leads to structural differences between chitosan and PNAG in solution where chitosan adopts a linear conformation and PNAG forms a helical structure.[31] Based upon the different architectures of the polysaccharides in solution, the chitosan probe should be an ideal negative control for our targeted-proteomics approach. The synthesis of chitosan probes follows largely the same protocol employed for the type I and type II probe

design. Using these controls should allow for differentiation between specific PNAG binding proteins and those that simply bind non-specifically to GlcNAc and GlcN.

This type of proteomics-based approach using diazirines as the main photoactive group have been well documented in the literature. First, a study that was attempting to understand the mechanism of action of fatty acid esters of monogalactosyldiacylglycerol (MGDG), used the diazirine as a crosslinker to determine what proteins bind to it.[32] MGDG's have anti-tumor, anti-viral, and anti-inflammatory properties, which make them attractive drug targets.[33] The modified MGDG with the diazirine was incubated in cell lysate and bound proteins were isolated and run on an SDS-page gel, stained with silver, and the most intense bands were sent for LC/MS-MS analysis.[32] Toll-like-receptor 4 was identified to be the major protein that bound to the probe and later it was determined that MGDG is an inhibitor of TLR4, which explains the anti-inflammatory effects of MGDG's.[32] Also, diazirines have been used to identify proteins that bind to pseudomonas quinoline signal (PDS), a virulence factor in the QS pathway of *P. aeruginosa*.[34] A modified PDS with a diazirine was incubated with cell lysate and enzymes were captured that interacted with the modified probe.[34] Captured proteins included lipopolysaccharide biosynthesis enzymes and proteins essential for virulence.[34] Overall, these studies indicate the power of diazrine crosslinkers and proteomics techniques involving carbohydrates and bacteria.

In this thesis I describe our synthesis and characterization of PNAG oligosaccharides, the preparation of diazarine modified levulinic acid, and synthesis

of the bifunctional linker. Work is still underway to establish an optimal methodology to link both diazirine containing compounds to the PNAG oligosaccharides.

Preliminary Results and Discussion:

Synthesis of PNAG and chitosan:

We started the synthesis of both PNAG probes by employing an acid reversion process to form the *N*-acetylglucosamine polymer **6** (**Scheme 2**). This process has been previously described[26], and is a protecting group-free method to prepare PNAG derivatives more efficiently than other chemical approaches, such as various one-pot synthesis[35], solid phase synthesis[36,37], or convergent approaches[37,38], and can provide more material than direct isolation of PNAG from *E. coli* cell cultures. We carried out the acid reversion process by dissolving *N*-acetylglucosamine in 70% HF-pyridine for up to a week, two days longer than the published procedure of 5 days.[26] A greater yield of the n>5 polymer was observed when the solution was stirred for 7 days as compared to 5 days. Also, the higher molecular weight (n>5) fraction after 7 days contained n = 8–12 oligosaccharides that were not observed after 5 days. Size exclusion chromatography on a bio-gel P6 column was used to separate the reaction products into three fractions based on their molecular weight. A high molecular weight fraction (n>5, **18%**), a medium weight fraction (n=3-5, **40%**) and a low molecular weight fraction (n < 3 **37%**) were isolated. However, we were unable to purify the products down to a single length size. In the future, additional size exclusion chromatography steps are likely required to isolate a uniform polymer of desirable size.

While the synthesis of compound **6** proved successful, the deacetylation of **6** to give compound **3** proved a challenge (**Scheme 2**). In *E. coli,* roughly 20% of the monosaccharides in PNAG are deacetylated[39], and we wanted our probes to mimic native PNAG as much as possible. Initially, we attempted the saponification of **6** in 10M NaOH, a strategy employed previously by others[26,40]. However, after many attempts, this approach proved unsuccessful. We hypothesized that the free anomeric hydroxyl group was interfering with the deacetylation, as hydroxide could be attacking this position over the acetyl groups. Lending further support to our theory, in the work by Nitz, the anomeric position was protected by using an *O*-alkyl-*N*-methyl hydroxylamine derived linker, which prevented any side reaction of NaOH.[26] Thus, we attempted to use N,O-dimethyl hydroxylamine to protect the reducing-end GlcNAc [41], of compound **6** to generate compound **7** (**Scheme 3**). Once the anomeric protecting group was

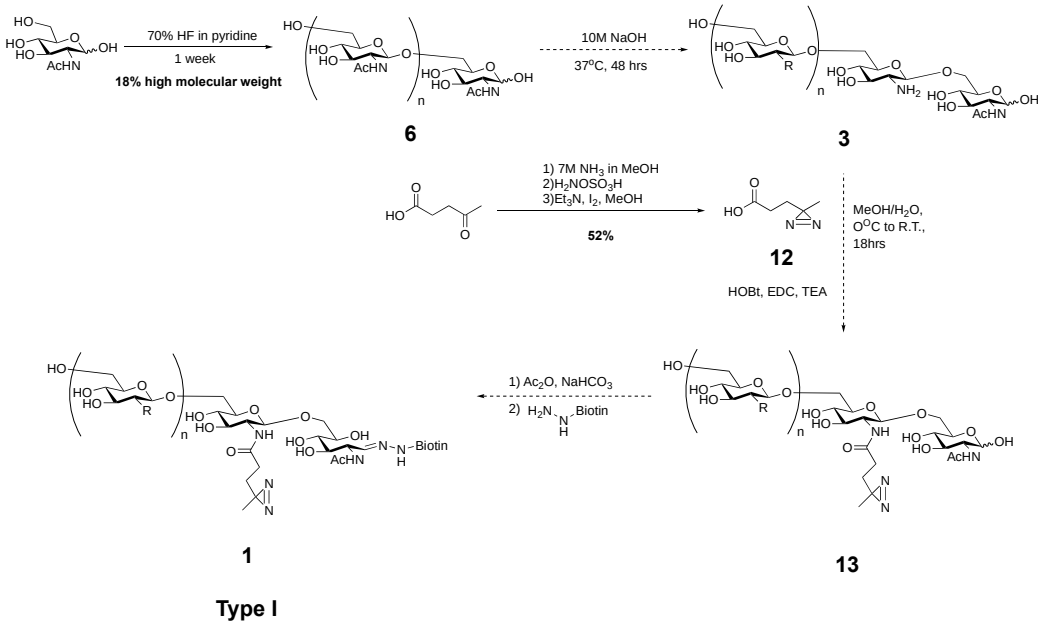

Scheme 2: Initial synthetic plan for type I probes. The chitosan probe lacks the deacetylation step.

installed, the PNAG oligomer could be deacetylated using the same basic conditions to form compound **8**, then deprotected to give compound **3.**[41] However, attachment of the protecting group proved unsuccessful, possibly due to the poor solubility of PNAG under the conditions needed to solubilize the protecting group. After the failed attempts to deacetylate PNAG, a new approach was developed (**Scheme 4**).

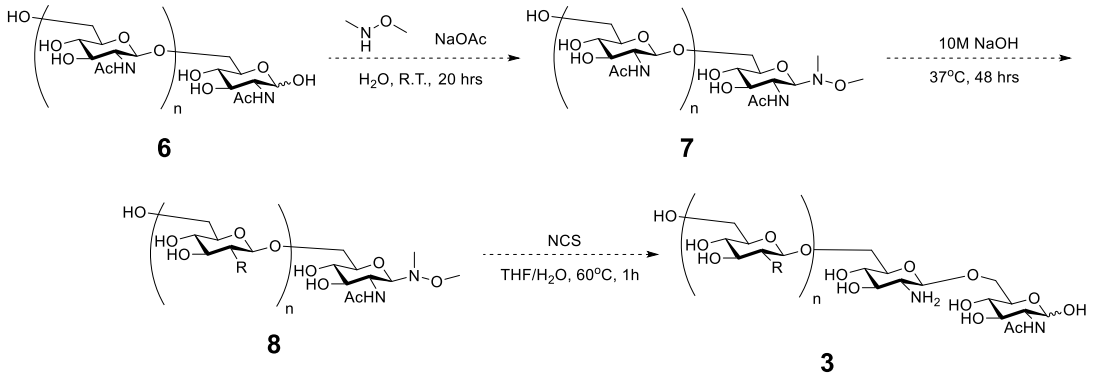

Scheme 3: First attempt to work around the PNAG deacetylation problem.

Our new strategy to make PNAG involved replacing *N*-acetylglucosamine in the first step, with a *N*-phthalimide-protected glucosamine **9** (**Scheme 4**).[42] The protected glucosamine **9**, will be employed as the monomer in the acid reversion reaction to make *N*-phthalimide-protected poly-glucosamine **10**. The phthalimide protecting group will be removed using hydrazine hydrate, a common method to remove phthalate protecting groups, to give compound **11**. Currently, the first step in this new method has proven successful, as compound **9** was isolated by reacting glucosamine HCl with phthalic anhydride in a sodium bicarbonate solution (**38%**). The next two steps in the process should go smoothly as well, and the removal of the phthalate from PNAG analogues has been previously reported.[43]

The synthesis of the chitosan-derived negative control probes started with commercially available high molecular weight chitosan. A number of methods to make low molecular weight chitosan oligosaccharide fragment (n=5–8) from high molecular weight chitosan (~ 50,000-190,000 Da) were attempted, including sonication[44], molecular sieve facilitated hydrolysis[45], and finally treating with concentrated HCl,[46] which proved to be the most effective method. High molecular weight chitosan was dissolved in concentrated aqueous HCl and heated to ~70ºC for 1.5 hrs, and the reaction was quenched by adding 10 M NaOH until the pH reached 7. However, the main challenge with this synthesis was the removal of the salts generated after the reaction was quenched. Most of the salts were removed by removing as much of the aqueous solution as possible by rotary evaporation, which caused salts to crash out of solution. Then the concentrated solution containing the desired fragments was decanted to separate the salts. More salts were removed on the FPLC when purifying the fragments further. However, after various attempts to remove the salts, there were some present in the fractions collected after FPLC.

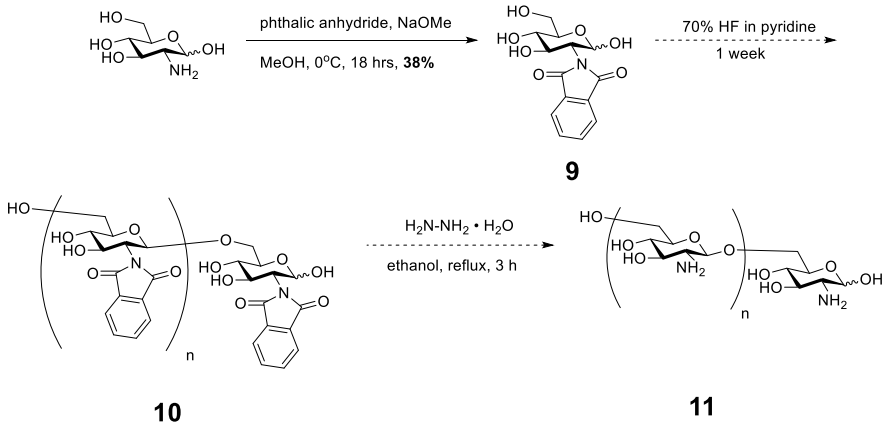

Scheme 4: Revised synthesis of PNAG to circumvent issues with deacetylation. This process removes the deacetylation step all together and relies on a N- deprotection strategy that has been used with PNAG in the literature.

Synthesis of type I probe with PNAG and chitosan:

The synthesis of the type I probe for PNAG and chitosan started with the synthesis compound **4** (**Scheme 1**). The synthesis was carried out by dissolving levulinic acid in 7M NH_3 in methanol, along with hydroxylamine-O-sulfonic acid, followed by iodine titration to yield compound **12** (**52%**) (**Scheme 2**)[27]. This is more technically simple than using than liquid NH_3[29], which can also be employed to make the diazirine functional group. Using NH_3 in methanol did not affect the yield of compound **12**, as the yield obtained was in line with what is reported in the literature. With compound **12** in hand, we attempted to react it with purified chitosan oligomers using an EDC amide coupling using a sub stoichiometric ratio of compound **12** relative to the chitosan oligomers to attach on average a single **12** per chitosan oligomer to give the chitosan analogue of compound **13 (Scheme 2).**[27] We chose to employ an EDC coupling as the amide is formed in one step and reacts selectively with the free amine, ignoring the unprotected hydroxyl groups of the chitosan/PNAG oligosaccharide. However, after a few attempts, this coupling was unsuccessful, mainly due to the poor solubility of chitosan in methanol/water. We were unable to attempt the EDC coupling with PNAG as we were unable to deacetylate our synthesized PNAG (compound **6**) as described previously.

To circumvent the solubility issues, we decided to implement an amide coupling strategy that is known to work well with chitosan in aqueous conditions and should be applicable to PNAG as well (**Scheme 5**). This strategy involves forming a N-hydroxysuccinimide ester from compound **12** to make compound **4** using a previously reported procedure[28]**,** then reacting compound **4** in acidic aqueous

conditions with compound **11** to form an amide with the free amine (compound **13a**, **Scheme 5**)[47]. Once the amide bond is formed, the next steps in the synthesis can be carried out, including acetylation and biotinylation to form the completed chitosan and PNAG probes (i.e. compound **1**, **Scheme 1**).[48]

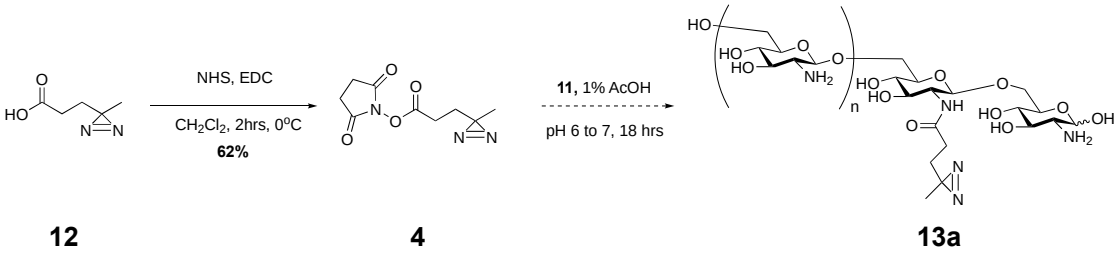

Scheme 5: Synthesis of the N-hydroxysuccinimide ester of compound **12** to form compound **13a**.

Synthesis of type II probe with PNAG and chitosan:

We chose to use 1-hydroxyhept-6-yn-3-one (compound **17**) as a starting material to synthesize the bifunctional linker (compound **5**, **Scheme 1**) as it has the required functional groups necessary for creating our probe (**Scheme 6**). Compound **17** contains a primary hydroxyl group that can be further functionalized, a terminal alkyne that can be used for copper-catalyzed click reactions, and central ketone equally spaced between the other two functional groups, which can be converted into a diazirine.

We initially purchased compound **17** to use in the synthesis of the final linker; however, due to its high cost (over $100 a gram) and limited availability from common chemical manufacturers we also sought to synthesize **17** in house. Compound **17** could be readily prepared using established literature methods (**Scheme 6**).[49] First, ethyl acetoacetate is allowed to react with two equivalents of

LDA followed by the addition of propargyl bromide to form compound **14**.[49] Then, the ketone is protected as the ketal using ethylene glycol to give compound **15**. The ester of **15** is then reduced with $LiAlH_4$ to generate the primary alcohol **16**.[49] The ketal is then removed under acidic conditions to yield compound **17**.[49] So far, only the first step to form compound **16** in 30% yield has been completed. The yield was low but may be improved following a new literature protocol from 2019, which obtained better yield with optimized conditions.[50]

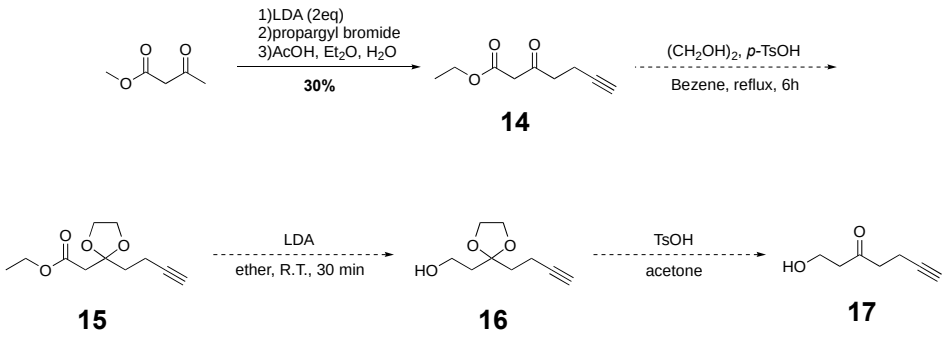

Scheme 6: Synthesis of 1-hydroxyhept-6-yn-3-one, the starting bifunctional linker for strategy 2.

Our initial strategy to prepare the type II probe began by synthesizing the bifunctional linker (compound **5, Scheme 7**) by forming the Boc-protected hydroxylamine (compound **20**) from a tosylate-primed intermediate (compound **18**).[26] Then, the diazirine would be formed (compound **21**) using a similar approach used to form the diazirine on levulinic acid,[27] and the hydroxylamine would be deprotected using TFA to yield compound **5**.[26] Out of this initial plan, the only step that was successful was the formation of compound **18,** which was isolated in a **64%** yield, in line with the literature.[51] The reaction of compound **18** with synthesized Boc-protected N-methyl hydroxylamine (compound **19, 69**%)[52] to generate the Boc-protected N,O substituted hydroxylamine **20** was unsucessful.[26] A possible reason for

the failure of this strategy could be that the hydride was deprotonating the alpha carbons on either side of the ketone or the terminal hydrogen on the alkyne, as the pKa's of these groups are around 20-25.

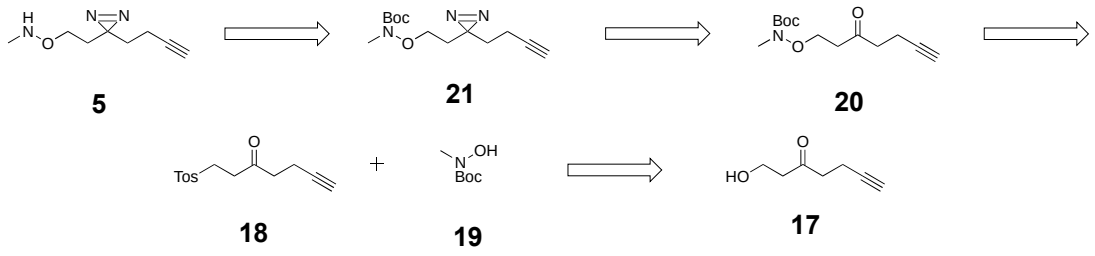

Scheme 7: Retrosynthetic analysis of the original strategy to achieve the bifunctional linker that will react with PNAG and chitosan.

In an attempt to circumvent this problem, we proposed a new synthetic route to prepare **20** using a Mitsunobu reaction (**Scheme 8**). After attempting the reaction at room temperature without success, we found that reacting compound **17** and **19** with PPh_3 and DIAD at 45ºC, gave compound **20** in a moderate yield (**40%**).[53] This approach also required on fewer steps than our previous route by directly conjugating compound **17** and **19** instead of making the intermediate **18**. Compound **20** was then treated following the previously described method to form the diazirine **21**. While formation of the diazirine proved successful, the hydroxylamine was lost during the reaction. We therefore decided to first convert the ketone of **17** to the diazirine to give **22** in **31%** yield, followed by the Mitsunobu reaction with compound **19** to yield **21** in **41%** yield (**Scheme 9**). The Boc group was then successfully removed using TFA to form compound **5** (**27%**). Next, the conjugation of compound **5** with compound **11** to make the thermodynamically stable β-glycoside (compound **23**) was attempted without success.[26] This reaction could have failed for two reasons. First, the

solubilities of the bifunctional linker and PNAG are not compatible in aqueous conditions. Second, and more likely, is that the equilibrium constants of the reaction between the anomeric position and the N-methyl hydroxylamine is low, and 1,4-diaminobenzene may need to be employed as a catalyst to speed up the reaction.[53,54] The final steps in the synthesis to make the type II probes for PNAG (compound **2**) and chitosan will be acetylation of the free amines by using acetic anhydride in excess followed by the copper-catalyzed click reaction with the terminal alkyne of the linker and azide-PEG_3-Biotin.[48] Overall, we predict that our revised synthesis will lead to the production of the type II PNAG and chitosan probes.

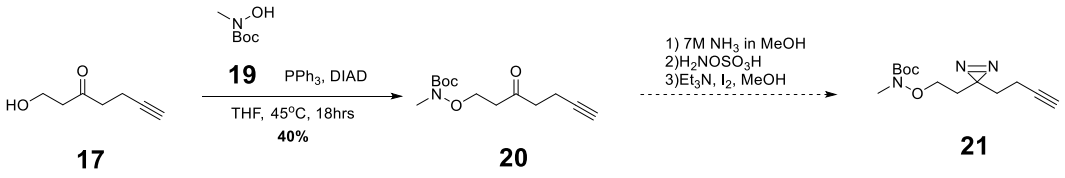

Scheme 8: Initial strategy employing the mitsunobu reaction.

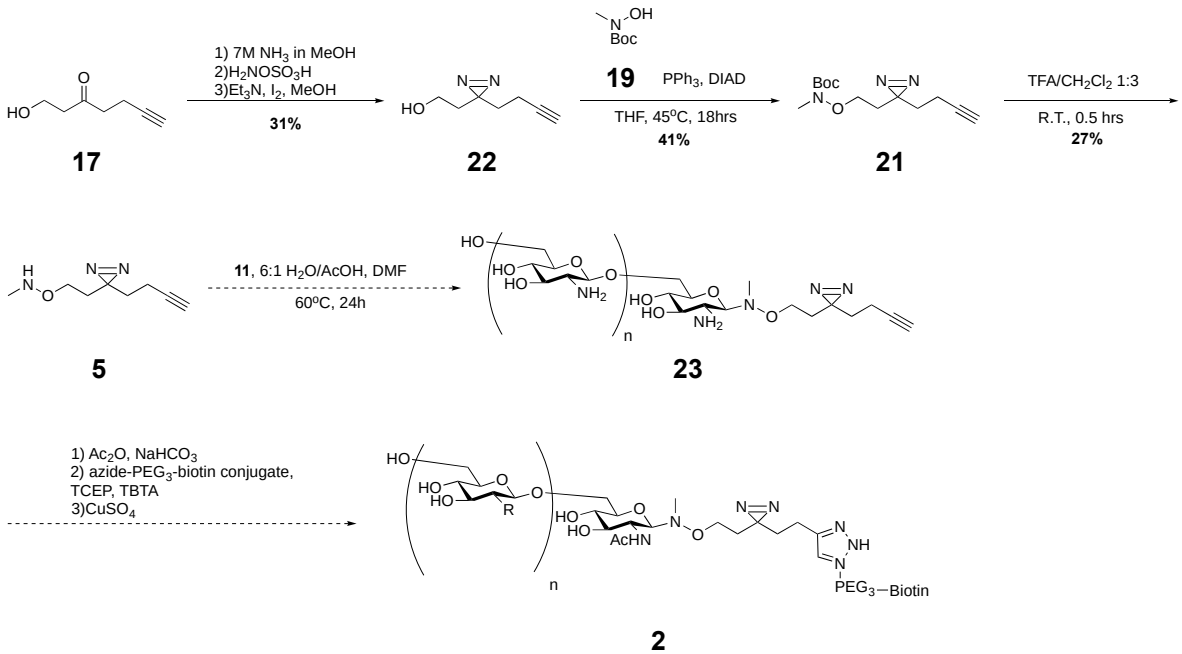

Scheme 9: Current strategy to couple the bifunctional linker **5** to PNAG and chitosan to form the type II probe.

Conclusions and Future Directions:

The main challenges with the synthesis of the type I and type II PNAG and chitosan probes was the deacetylation of PNAG and the coupling of both diazirine probes. To solve the PNAG deacetylation problem, a new synthesis was outlined where the free amine of glucosamine was protected with phthalic anhydride to create the new monomer **9** to be used in the acid-reversion reaction to produce the PNAG backbone (compound **10**). The phthalaminde protecting group can then be easily removed so that all amines in the PNAG background are free to accept compound **4** to generate compound **13**. This type of amide coupling to form the type I probes is commonly used and is known to work well with chitosan and should be adapted relatively easily to PNAG.

The synthesis of the bifunctional linker used in the type II probe was more challenging as the starting bi-functional linker **17** had to be synthesized. After troubleshooting problems coupling the *N*-Boc-*N*-methyl hydroxylamine **19** to compound **17**, we settled on using a mitsunobu reaction. The final challenge with synthesizing the type II probes will be conjugating the bifunctional linker **22** with the anomeric position of PNAG or chitosan. Recent literature suggests that this reaction can be accelerated with the use of a 1,4-diaminobenzene catalyst.

The proposed enhancements to the synthesis of the type I and type II probes should be relatively straightforward as most of the proposed changes have literature precedent. An estimated time frame to synthesize the type I and type II PNAG and chitosan probes would be 2 months. Two weeks would be needed to produce enough of compounds **11** and chitosan oligomers and another two weeks to complete the

synthesis of **4** and **17**. Finally, two weeks would be needed to complete the conjugation of compounds **4** or **17** with **11** and chitosan oligomers and the final two weeks would be used as a buffer in case any issues arose with the previously outlined steps. Following completion of the synthesis, the protein capture experiments using *E. coli* lysate and the characterization of any PNAG binding proteins is expected to take another 2 months, for an estimated completion of the project in 4 months. Any PNAG binding proteins identified using this approach will be investigated in greater detail to establish their function in PNAG dependent biofilm formation. If we are able to identify and then block specific PNAG binding proteins this may provide a new avenue to disrupt and prevent biofilm growth. Additionally, we can utilize our probes in other species of biofilm-forming bacteria that use PNAG in their EPS to see if there are any similarities in the types of proteins that associate with PNAG between species.

Experimental

General:
Compounds were used as received from Sigma Aldrich without modification. All solvents used were Sure-Seal solvents unless otherwise noted. TLC was performed on silica at ambient temperature. Silica gel 60 was used as the stationary phase for flash chromatography. All ^{1}H NMR spectra were taken using a Bruker Advance 400 MHz Fourier Transform Nuclear Magnetic Resonance Spectrometer. Abbreviations for spectra: s = singlet, br = broad singlet d = doublet, t = triplet, q = quartet, quin = quintet, dd = doublet of doublets, dt= triplet of doublets, m = multiplet.

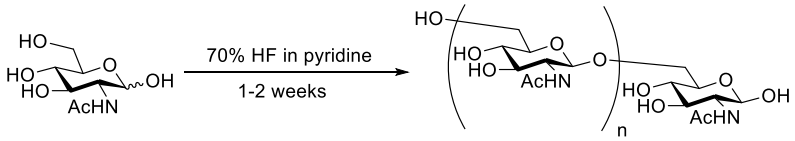

6

Poly-(1→6)-β-*N*-acetyl-D-glucosamine (PNAG) (6). *N*-Acetyl-D-glucosamine (2.00 g, 9.04 mmol) was added to a polypropylene conical tube, followed by 1.40 mL of HF (~70% in 30% pyridine, Sigma Aldrich). The contents were stirred for 7 to 14 days and were subsequently quenched through the addition of a slurry of calcium carbonate (6.00 g) in ice until the evolution of gas ceased (~30 min). The suspension was poured over celite and washed with water which yielded a pale yellow filtrate. The filtrate was concentrated *in vacuo* and filtered through 3 separate C18 silica columns (5.0 cm x 2.5 cm). Filtrate from the C18 columns were concentrated again *in vacuo* and injected onto a Bio-Gel P4 size exclusion column (5.0 cm I.D. x 70 cm, 40-90 µm particle size). MilliQ water was used as the eluent at 0.5 mL/min and column progress was monitored at 215 nm. Fractions with similar elution times were combined, concentrated *in vacuo* to give **6** as an off white solid (122 mg, n ≥ 5; 18% yield). The product distribution was characterized using MALDI-TOF MS using THAP as the matrix. *m/z* (MALDI) major peaks: 1056.23 n=5; 1259.34 n=6; 1462.42 n=7; 1665.50 n=8; 1868.58 n=9; 2071.65 n=10.

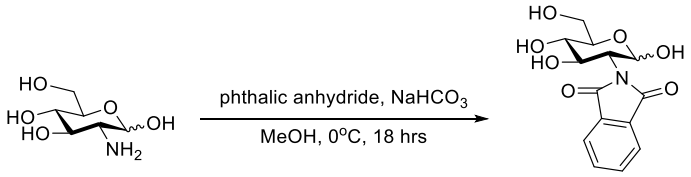

9

2-((2*R*,3*R*,4*R*,6*R*)-2,4,5-trihydroxy-6-(hydroxymethyl)tetrahydro-2*H*-pyran-3-yl)isoindoline-1,3-dione (9). A solution of D-glucoseamine HCl (5.39 g, 25.0 mmol), phthalic anhydride (3.70 g, 25.0 mmol), and sodium bicarbonate (4.20 g, 50.0 mmol) was stirred for 18 hrs at room temperature. The dark orange solution was acidified to

pH 2 with 2 M HCl, which after 5 min, caused a white suspension to form. The precipitate was washed with water and dried using a Buchner funnel to yield the desired compound as a white solid. (2.95 g, **38%**) δ_H (400 MHz; $CDCl_3$) 7.97-7.95 (dd, 1H, *J*=1.0, 7.5 Hz), 7.68-7.58 (m, 2H), 7.54-7.51 (dd, 1H, *J*=1.0, 7.5 Hz), 5.34 (d, 1H, *J*=3.5 Hz), 4.09-4.04 (dd, 1H, *J*=3.5 ,10.6 Hz), 3.91-3.76 (m, 4H), 3.53 (t, 1H, *J*= 9.5 Hz)

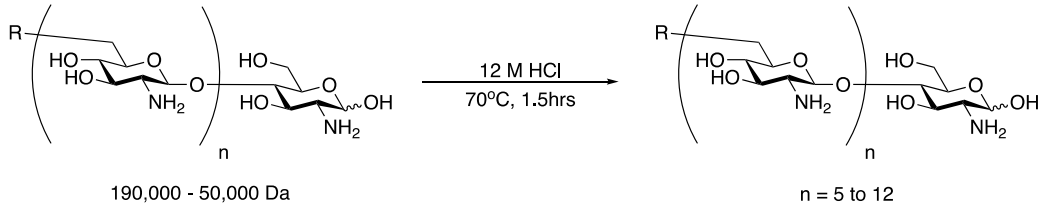

Chitosan Oligomer Production. Chitosan (2.00 g) was placed in a 1-neck round bottom flask along with a stir bar. Next, 100 mL of neat HCl poured into the flask and the flask was submerged in an oil bath at 68.5°C for 1.5 hrs with the top open to allow HCl to vent into the fume hood. After heating, the cloudy brown solution inside the flask was quenched by placing it in a dry-ice acetone bath for 10 min. The pH was adjusted to 3-4 with 10 M NaOH while the flask was in the dry ice/acetone bath to prevent overheating. During addition of NaOH, a precipitate could be seen forming. Next, activated charcoal was added and the solution was filtered through a Millipore, 22 µm filter using a Buchner funnel. The resulting clear-yellow filtrate was concentrated to ~50 mL *in vacuo*. Once condensed, the solution was brought to pH 8-9 and turned from clear-yellow to clear-brown and the solution was filtered through 2 C18 columns (5.0 cm x 2.5 cm) and re-concentrated *in vacuo*. A 6 mL aliquot was placed on the size exclusion column Bio-Gel P4 size exclusion column (5.0 cm I.D. x 70 cm, 40-90 µm particle size) using MilliQ water as the eluent at 0.5 mL/min while monitored for absorbance at 215 nm. MALDI:1049.22 n=6, 1210.27 n=7, 1371.31 n=8, 1532.35 n=9, 1693.39 n=10.

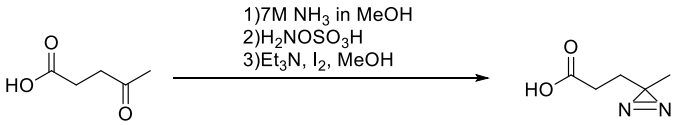

12

4,4-azo-pentanoic acid (12). A round bottom flask was charged with a stir bar and capped with a septum that had a syringe with a balloon attached. Next, levulinic acid (700 µL, 6.80 mmol) was injected into the flask and the flask was submerged in an ice bath for 5 min. Then, 7 mL of 7 M ammonium hydroxide in MeOH (Sigma

Aldrich, 47.6 mmol) was added and the solution was stirred in the ice bath for 3 hrs. Hydroxylamine O-sulfonic acid (885 mg, 7.82 mmol) in 7 mL MeOH was then added dropwise. The reaction was kept stirring while slowly warming to r.t. in the ice bath for 18 hrs. Ammonia was removed from the solution by gently blowing air over the solution for 1 hr. The white precipitate that had formed was removed by pouring the mixture over Celite and the precipitate was washed several times with cold MeOH, leaving a pale yellow filtrate. The filtrate was concentrated *in vacuo*, covered with aluminum foil, and submerged in an ice bath for 5 min. Next, 1.50 mL of TEA (10.3 mmol) was added and the flask sat in the ice bath for 5 min while the mixture was stirred. Then, making sure to limit exposure to light, iodine chips were slowly added to the mixture until the solution remained a persistent dark brown (about 1 g of iodine) and the solution was stirred in the ice bath for an hour. The mixture was poured into a separatory funnel followed by 10 mL of EtOAc and 10 mL 1 M HCl to wash the organic layer. The aqueous layer was extracted with 3x20 mL of EtOAc. The organic layers were combined and washed with 3x15 mL of sodium thiosulfate hexahydrate and 30 mL brine then dried over Na_2SO_4. The solvent was removed by rotary evaporation resulting in a yellow-orange oil and stored at -20°C (0.460 g, **52%**). δ_H (400 MHz; $CDCl_3$) 9.81 (br, 1.5H), 2.16 (t, 2H, *J*=8 Hz), 1.63 (t, 2H, *J*=8 Hz), 0.96 (s, 3H).

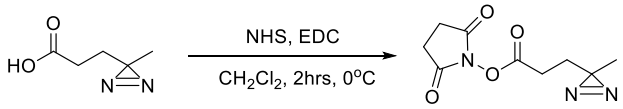

12 **4**

succinimidyl 4,4-azipentanoate (4). Compound **12** (0.350 g, 2.70 mmol), N-hydroxysuccinimide (0.34, 2.97 mmol), and EDC hydrochloride (0.570 g, 2.97 mmol) were dissolved in 10 mL anhydrous methylene chloride at 0°C. The solution was then stirred at room temperature for 2 h and the solution had turned to olive green. The solution was then diluted with 10 ml of methylene chloride and washed 3x25 mL of dH_2O and 1x25 mL brine. The organic layer was dried over $MgSO_4$ and concentrated by rotary evaporation to yield an orange solid. δ_H (400 MHz; $CDCl_3$) 2.87 (s, 4H), 2.51 (t, 2H, *J*=8Hz), 1.79 (t, 2H, *J*=8.0 Hz), 1.06 (s, 3H).

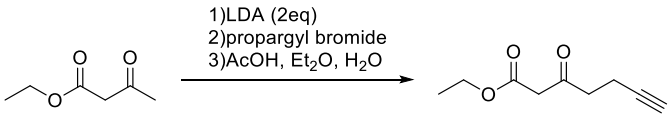

14

ethyl 3-oxohept-6-ynoate (14). A solution of 2 M LDA in THF and hexanes (Sigma-Aldrich) (12.7 mL, 25.4 mmol) was added to a pre-chilled round bottom flask equipped with a stir bar. Next, ethyl acetoacetate (16.2 mL, 12.68 mmol) was added and upon addition, a violent reaction and off-gassing could be seen taking place. The solution was then stirred and immediately turned from a clear-dark orange to a dark

red. The solution was stirred for 30 min, then propargyl bromide (9.61 ml, 12.68 mmol) was added and the solution was stirred for an additional hour in the ice bath. The addition of the propargyl bromide turned the solution from a dark red to a clear vivid-orange and some bubbling was also observed. After 1 h, the reaction was quenched with glacial acetic acid (14.5 mL, 25.36 mmol) which caused a precipitate to form. Equal portions of DI H_2O and diethyl ether (75 mL) were added to the organic layer. The aqueous layer was separated from the organic layer and extracted with 50 mL diethyl ether. The organic layers were combined and washed with 50 mL of brine and dried over sodium sulfate. Excess solvent was removed *in vacuo* and the dark orange oil that was left was stored at 0^oC until further use. Optimal column conditions (90% hexanes, 10% ethyl acetate, vanillin stain, Rf = 0.28) were determined by TLC. The crude oil was placed on a 30 g silica column from Biotage and run on a Biotage automated column using the above TLC conditions. The column progress was monitored by UV vis (200-400 nm) and appropriate fractions were combined and condensed using rotary evaporation to yield a yellow oil (600 mg, **28%**). δ_H (400 MHz; $CDCl_3$): 4.12 (q, 2H, *J* = 6.5 Hz), 3.90 (d, 2H, *J* = 9.2 Hz), 2.75 (t, 1H, *J* = 7.2 Hz), 2.39 (t, 1H, *J* = 6.5 Hz), 2.19 (s, 1H), 1.91 (t, 1H, *J* = 19.2 Hz), 1.21 (t, 3H, *J* = 7.2 Hz).

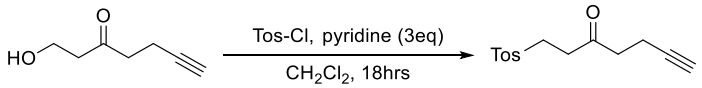

10

3-oxohept-6-yn-1-yl 4-methylbenzenesulfonate (18). A round bottom flask was charged with a stir bar and purged with argon followed by the addition of 1-hydroxyhept-6-yn-3-one (200 mg, 1.59 mmol), 4-toluenesulfonyl chloride (465 mg, 2.38 mmol), pyridine (385 μL, 4.76 mmol), and 5 mL of dry methylene chloride. The mixture was placed in an ice bath and left to stir for 20 h under argon. Next, the mixture was poured into a separatory funnel along with 10 mL DI H_2O. The aqueous layer was extracted with 10 mL of methylene chloride and the combined organic layers were dried over Na_2SO_4 and residual solvent was removed *in vacuo*. The optimal TLC conditions to give an Rf = 0.37 were 70% hexanes, 30% ethyl acetate. The yellow oil obtained was placed on a Biotage silica gel column and run on a Biotage automated column chromatography system. Fractions containing the product were combined and solvent removed using rotary evaporation to give a yellow oil (286 mg, **64%**). δ_H (400 MHz; $CDCl_3$) 7.78 (d, 2H, *J* = 8 Hz), 7.36 (d, 2H, *J* = 8 Hz), 4.28 (t, 2H, *J* = 6 Hz), 2.83 (t, 2H, *J* = 6 Hz), 2.65 (t, 2H, *J* = 7.2 Hz), 2.44 (m, 5H), 1.942 (s, 1H).

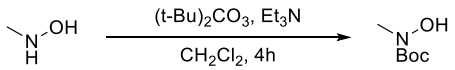

19

***tert*-butyl methyl((3-oxohept-6-yn-1-yl)oxy)carbamate (19).** A round bottom flask was charged with a stir bar and purged with argon for 10 min. Next, N-methyl hydroxylamine (927 mg, 11.1 mmol) and di-tertbutyl decarbonate (1940 mg, 8.88 mmol) were added to the flask and dissolved in approx 32 mL of dry methylene chloride. Triethylamine was then added (1.95 mL, 13.8 mmol) and the reaction was stirred for 18 h under argon atmosphere. After stirring overnight, the clear, colorless solution was washed with 0.1 M Na_2SO_4 (3x30 mL) followed by brine (2x30 mL). The organic layer was dried with sodium sulfate and the solid was removed by gravity filtration. The excess organic solvent was removed *in vacuo* to give a clear, magenta oil. A proton NMR was taken of the oil in $CDCl_3$. (897 mg, **69%**). δ_H (400 MHz; $CDCl_3$) 3.09 (s, 3H), 1.41 (s, 10H).

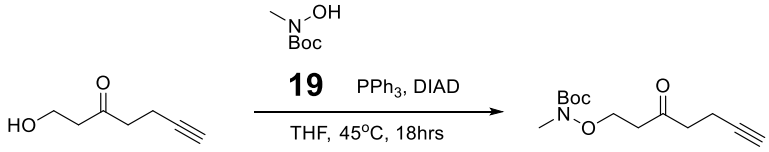

17 **20**

***tert*-butyl methyl((3-oxohept-6-yn-1-yl)oxy)carbamate (20).** A round bottom flask was charged with a stir bar along with triphenylphosphine (375 mg, 1.43 mmol). The flask was capped with a septum and purged with argon for 10 min. Then, 4 mL of dry THF was added to the flask and the resulting solution was stirred for 5 min. Next, compound **17** (120 μL, 0.95 mmol) was added, followed by compound **19** (260 μL, 1.90 mmol). The flask was submerged in an ice bath for 1 min, then DIAD (350 μL, 1.76 mmol) was added dropwise. The flask was then removed from the ice bath and was allowed to warm to RT for 10 min while stirring. Once warmed to RT, the flask was submerged in an 50°C oil bath for 18 hrs. After heating, excess solvent was *in vacuo*, resulting in an oily yellow residue. The residue was dissolved in dichloromethane and a TLC was taken in 30% ethyl acetate, 70% hexanes and stained with ninhydrin, which showed that the product had a Rf = ~0.55. The residue was run on a Biotage silica gel column on a Biotage automated column system with the respective TLC plate settings. Appropriate fractions were isolated and condensed using rotary evaporation. Proton NMR in $CDCl_3$ showed that unreacted compound **8** was still present after chromatography. The residue was then dissolved in 15 mL of diethyl ether and washed with 20 wt% sodium bisulfate solution (3x10 mL), 0.1 M NaOH (2x10 mL), and brine (1x10 mL. The organic layer was further dried using sodium sulfate and excess solvent was removed by rotary evaporation. A proton NMR of the oil was taken in $CDCl_3$ (243 mg, **41%**). δ_H (400 MHz; $CDCl_3$) 4.1 (t, 2H, *J*=6 Hz), 3.03 (s, 3H), 2.70 (t, 4H, *J*=6 Hz), 2.44 (t, 2.5H, *J*=2.4Hz), 2.14 (s, 0.5H), 1.92(t, 1H, *J*=2.4Hz), 1.46 (s, 11H).

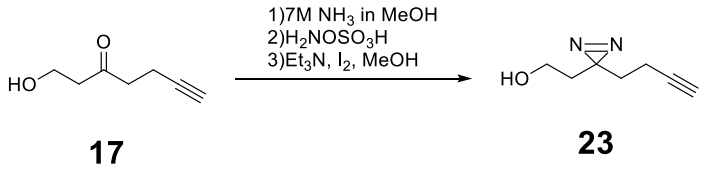

17 **23**

2-(3-(but-3-yn-1-yl)-3*H*-diazirin-3-yl)ethan-1-ol (23). Compound **17** (250 mg, 1.98 mmol) was added to a round bottom flask equipped with a stir bar. The flask was sealed with a septum and placed in an ice-water bath for 5 min. A balloon was attached to the septum to maintain pressure within the flask. Next, 7M ammonium hydroxide in methanol (1.98 mL, 13.87 mmol) was injected into the flask and the flask was left in the ice bath for 3 hrs with stirring. A solution of hydroxylamine-O-sulfonic acid (258 mg, 2.28 mmol) in a minimal amount of methanol was then injected dropwise and the resulting solution was stirred for 18 h while it warmed to RT. After stirring overnight, a white suspension had formed in the flask. The precipitate was separated from the pale-yellow solution by syringe filter and the precipitate was washed with cold methanol. The solution was concentrated *in vacuo*, leaving a yellow oil residue. The residue was then dissolved in 2 mL methanol and transferred to a round bottom flask covered in aluminum foil and placed in an ice bath for 5 min while stirring. Triethylamine (420 µL, 3.01 mmol) was added and the flask was stirred in the ice bath for another 5 min. A solution of iodine (654 mg, 2.57 mmol) in a minimal amount of methanol was added dropwise until the color of the solution was persistently purple. The flask was kept in the ice bath for an additional hour while stirring. Afterwards, the reaction was diluted in 10 mL ethyl ether, followed by washing with 10 mL brine. The brine was washed with diethyl ether (3x10 mL) and the combined organic layers were dried with sodium sulfate. Excess solvent was removed *in vacuo*, resulting in a yellow oil. The oil was run on a Biotage silica gel column that was used with a Biotage automated column system with 80% hexanes, 20% ethyl acetate. Appropriate fractions (Rf = 0.25, plate stained with vanillin) were collected, combined, and condensed *in vacuo* to yield a pale yellow oil (90 mg, **33%**). δ_H (400 MHz; $CDCl_3$): 3.46 (t, 2H, *J* = 6.4 Hz), 2.13 (br, 1H), 2.04-1.99 (m, 3H), 1.70-1.64 (m, 4H).

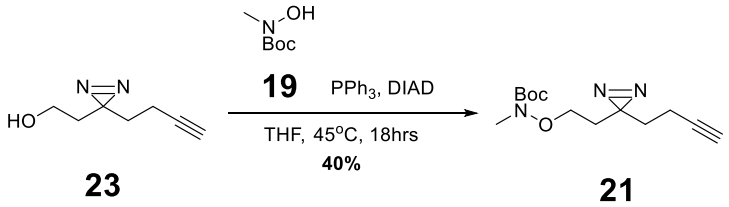

23 **21**

***tert*-butyl (2-(3-(but-3-yn-1-yl)-3*H*-diazirin-3-yl)ethoxy)(methyl)carbamate (21).** Compound **23** (90.0 mg, 0.71 mmol) was combined with triphenylphosphine (281 mg, 1.07 mmol) in a round bottom flask equipped with a stir bar. The flask was then purged with argon for 10 min, then 2 mL of THF was added and the stirring was

turned on. Next, Compound **19** (210 mg, 1.43 mmol, 2 eq) was added when the first two reagents had dissolved and the flask was placed in an ice bath for 5 min to cool. DIAD (267 mg, 1.32 mmol) was added dropwise and the flask was taken out of the ice bath after the addition was complete. The flask was then placed in an oil bath set at 45^{O}C overnight. A TLC was then taken of the crude in 70% hexanes and 30% ethyl acetate which gave an Rf = 0.68 for the target compound when stained with vanillin and ninhydrin. Next, 10 mL of diethyl ether was added to the organic layer and washed with 20 wt% potassium bicarbonate (10 x 3 mL) followed by 0.1 M sodium hydroxide (2 x 10 mL) and brine (1 x 10 mL). The organic layer was dried over sodium sulfate and the organic layer was condensed *in vacuo*, resulting in a yellow oil. TLC was performed with similar conditions as above on the yellow oil to confirm the removal of excess compound **9**. The crude oil was run through a Biotage silica gel column on a Biotage automated column system with the same TLC conditions used for this compound previously. Similar fractions were combined and condensed via rotary evaporation to yield a pale yellow oil (61 mg, **32%**). δ_H (400 MHz; $CDCl_3$): 3.77 (t, 1H, *J* = 6 Hz), 3.67 (t, 1H, *J* = 6 Hz), 3.09 (d, 3H, *J* = 6 Hz), 2.04-1.95 (m, 4H), 1.74-1.60 (m, 5H), 1.47 (d, 15H, 1.6 Hz).

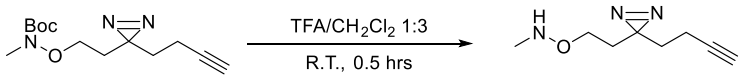

21 **22**

***O*-(2-(3-(but-3-yn-1-yl)-3*H*-diazirin-3-yl)ethyl)-*N*-methylhydroxylamine (22).** Compound **21** (60.0 mg, 0.22 mmol) was placed into a round bottom flask covered with aluminum foil and charged with a stir bar. Next, 0.33 mL (0.68 M) of TFA in dichloromethane (1:3) was added to the linker - the color of the solution became darker and bubbling was observed. The solution was stirred at RT for 30 min then 10 mL of diethyl ether was added to the flask. The organic layer was washed with saturated sodium bicarbonate (3x10 mL), dried over sodium sulfate, and filtered by gravity filtration. The organic solvents were removed by rotary evaporation to give a yellow oil. A ^{1}H NMR confirmed that the product had been formed but was impure (10 mg, **15%**). δ_H (400 MHz; $CDCl_3$): 3.60 (t, 2H, *J* = 6.4 Hz), 2.048-1.981 (m, 6H), 1.736-1.659 (m, 7H).

Bibliography

(1) Wingender, J.; Neu, T. R.; Flemming, H.-C. *Microbial Extracellular Polymeric Substances*; Springer-Verlag Berlin Heidelberg, 1999.

(2) Calfee, D. P.; Salgado, C. D.; Milstone, A. M.; Harris, A. D.; Kuhar, D. T.; Moody, J.; Aureden, K.; Huang, S. S.; Maragakis, L. L.; Yokoe, D. S. Strategies to Prevent Methicillin-Resistant Staphylococcus Aureus Transmission and Infection in Acute Care Hospitals: 2014 Update. *Infect. Control Hosp. Epidemiol.* **2014**, *35* (07), 772–796.

(3) Costerton, J. W. Bacterial Biofilms: A Common Cause of Persistent Infections. *Science* **1999**, *284* (5418), 1318–1322.

(4) Hall-Stoodley, L.; Costerton, J. W.; Stoodley, P. Bacterial Biofilms: From the Natural Environment to Infectious Diseases. *Nat. Rev. Microbiol.* **2004**, *2* (2), 95–108.

(5) Monroe, D. Looking for Chinks in the Armor of Bacterial Biofilms. *PLoS Biol.* **2007**, *5* (11), e307.

(6) Flemming, H.-C.; Wingender, J. The Biofilm Matrix. *Nat. Rev. Microbiol.* **2010**, *8* (9), 623–633.

(7) Petrova, O. E.; Sauer, K. Sticky Situations: Key Components That Control Bacterial Surface Attachment. *J. Bacteriol.* **2012**, *194* (10), 2413–2425.

(8) Watnick, P. I.; Kolter, R. Steps in the Development of a Vibrio Cholerae El Tor Biofilm. *Mol. Microbiol.* **1999**, *34* (3), 586–595.

(9) Danese, P. N.; Pratt, L. A.; Kolter, R. Exopolysaccharide Production Is Required for Development of Escherichia Coli K-12 Biofilm Architecture. *J. Bacteriol.* **2000**, *182* (12), 3593–3596.

(10) Tielen, P.; Strathmann, M.; Jaeger, K.-E.; Flemming, H.-C.; Wingender, J. Alginate Acetylation Influences Initial Surface Colonization by Mucoid Pseudomonas Aeruginosa. *Microbiol. Res.* **2005**, *160* (2), 165–176.

(11) Franklin, M. J.; Ohman, D. E. Identification of AlgF in the Alginate Biosynthetic Gene Cluster of Pseudomonas Aeruginosa Which Is Required for Alginate Acetylation. *J. Bacteriol.* **1993**, *175* (16), 5057–5065.

(12) Wozniak, D. J.; Wyckoff, T. J. O.; Starkey, M.; Keyser, R.; Azadi, P.; O'Toole, G. A.; Parsek, M. R. Alginate Is Not a Significant Component of the Extracellular Polysaccharide Matrix of PA14 and PAO1 Pseudomonas Aeruginosa Biofilms. *Proc. Natl. Acad. Sci.* **2003**, *100* (13), 7907–7912.

(13) Mayer, C.; Moritz, R.; Kirschner, C.; Borchard, W.; Maibaum, R.; Wingender, J.; Flemming, H.-C. The Role of Intermolecular Interactions: Studies on Model Systems for Bacterial Biofilms. *Int. J. Biol. Macromol.* **1999**, *26* (1), 3–16.

(14) Yan, J.; Sharo, A. G.; Stone, H. A.; Wingreen, N. S.; Bassler, B. L. *Vibrio Cholerae* Biofilm Growth Program and Architecture Revealed by Single-Cell Live Imaging. *Proc. Natl. Acad. Sci.* **2016**, *113* (36), E5337–E5343.

(15) Mack, D.; Fischer, W.; Krokotsch, A.; Leopold, K.; Hartmann, R.; Egge, H.; Laufs, R. The Intercellular Adhesin Involved in Biofilm Accumulation of Staphylococcus Epidermidis Is a Linear Beta-1,6-Linked Glucosaminoglycan: Purification and Structural Analysis. *J. Bacteriol.* **1996**, *178* (1), 175–183.

(16) Agladze, K.; Wang, X.; Romeo, T. Spatial Periodicity of Escherichia Coli K-12 Biofilm Microstructure Initiates during a Reversible, Polar Attachment Phase of Development and Requires the Polysaccharide Adhesin PGA. *J. Bacteriol.* **2005**, *187* (24), 8237–8246.
(17) Choi, A. H. K.; Slamti, L.; Avci, F. Y.; Pier, G. B.; Maira-Litran, T. The PgaABCD Locus of Acinetobacter Baumannii Encodes the Production of Poly-1-6-N-Acetylglucosamine, Which Is Critical for Biofilm Formation. *J. Bacteriol.* **2009**, *191* (19), 5953–5963.
(18) Cramton, S. E.; Gerke, C.; Schnell, N. F.; Nichols, W. W.; Tz, F. G. The Intercellular Adhesion (Ica) Locus Is Present in Staphylococcus Aureus and Is Required for Biofilm Formation. *INFECT IMMUN* **1999**, *67*, 7.
(19) Heilmann, C.; Schweitzer, O.; Gerke, C.; Vanittanakom, N.; Mack, D.; Götz, F. Molecular Basis of Intercellular Adhesion in the Biofilm-Forming Staphylococcus Epidermidis. *Mol. Microbiol.* **1996**, *20* (5), 1083–1091.
(20) Vuong, C.; Kocianova, S.; Voyich, J. M.; Yao, Y.; Fischer, E. R.; DeLeo, F. R.; Otto, M. A Crucial Role for Exopolysaccharide Modification in Bacterial Biofilm Formation, Immune Evasion, and Virulence. *J. Biol. Chem.* **2004**, *279* (52), 54881–54886.
(21) Little, D. J.; Pfoh, R.; Le Mauff, F.; Bamford, N. C.; Notte, C.; Baker, P.; Guragain, M.; Robinson, H.; Pier, G. B.; Nitz, M.; et al. PgaB Orthologues Contain a Glycoside Hydrolase Domain That Cleaves Deacetylated Poly-β(1,6)-N-Acetylglucosamine and Can Disrupt Bacterial Biofilms. *PLOS Pathog.* **2018**, *14* (4), e1006998.
(22) Little, D. J.; Li, G.; Ing, C.; DiFrancesco, B. R.; Bamford, N. C.; Robinson, H.; Nitz, M.; Pomes, R.; Howell, P. L. Modification and Periplasmic Translocation of the Biofilm Exopolysaccharide Poly- -1,6-N-Acetyl-D-Glucosamine. *Proc. Natl. Acad. Sci.* **2014**, *111* (30), 11013–11018.
(23) Bertozzi, C.; Kiessling, L. Chemical Glycobiology. *Science* **2001**, *291* (5512), 2357–2364. https://doi.org/10.1126/science.1059820.
(24) Tanaka, Y.; Kohler, J. J. Photoactivatable Crosslinking Sugars for Capturing Glycoprotein Interactions. *J. Am. Chem. Soc.* **2008**, *130* (11), 3278–3279.
(25) Bond, M. R.; Zhang, H.; Kim, J.; Yu, S.-H.; Yang, F.; Patrie, S. M.; Kohler, J. J. Metabolism of Diazirine-Modified *N* -Acetylmannosamine Analogues to Photo-Cross-Linking Sialosides. *Bioconjug. Chem.* **2011**, *22* (9), 1811–1823.
(26) Leung, C.; Chibba, A.; Gómez-Biagi, R. F.; Nitz, M. Efficient Synthesis and Protein Conjugation of β-(1→6)-d-N-Acetylglucosamine Oligosaccharides from the Polysaccharide Intercellular Adhesin. *Carbohydr. Res.* **2009**, *344* (5), 570–575.
(27) Bond, M. R.; Zhang, H.; Vu, P. D.; Kohler, J. J. Photocrosslinking of Glycoconjugates Using Metabolically Incorporated Diazirine-Containing Sugars. *Nat. Protoc.* **2009**, *4* (7), 1044–1063.
(28) Sun, R.; Yin, L.; Zhang, S.; He, L.; Cheng, X.; Wang, A.; Xia, H.; Shi, H. Simple Light-Triggered Fluorescent Labeling of Silica Nanoparticles for Cellular Imaging Applications. *Chem. - Eur. J.* **2017**, *23* (56), 13893–13896.
(29) Li, Z.; Hao, P.; Li, L.; Tan, C. Y. J.; Cheng, X.; Chen, G. Y. J.; Sze, S. K.; Shen, H.-M.; Yao, S. Q. Design and Synthesis of Minimalist Terminal Alkyne-

Containing Diazirine Photo-Crosslinkers and Their Incorporation into Kinase Inhibitors for Cell- and Tissue-Based Proteome Profiling. *Angew. Chem. Int. Ed.* **2013**, *52* (33), 8551–8556.
(30) Tolonen, A. C.; Haas, W. Quantitative Proteomics Using Reductive Dimethylation for Stable Isotope Labeling. *J. Vis. Exp.* **2014**, No. 89.
(31) Grachev, A. A.; Gerbst, A. G.; Gening, M. L.; Titov, D. V.; Yudina, O. N.; Tsvetkov, Y. E.; Shashkov, A. S.; Pier, G. B.; Nifantiev, N. E. NMR and Conformational Studies of Linear and Cyclic Oligo-(1→6)-β-d-Glucosamines. *Carbohydr. Res.* **2011**, *346* (15), 2499–2510.
(32) Liu, X.; Dong, T.; Zhou, Y.; Huang, N.; Lei, X. Exploring the Binding Proteins of Glycolipids with Bifunctional Chemical Probes. *Angew. Chem.* **2016**, *128* (46), 14542–14546.
(33) Halloran, M. W.; Lumb, J. Recent Applications of Diazirines in Chemical Proteomics. *Chem. – Eur. J.* **2019**, *25* (19), 4885–4898.
(34) Dandela, R.; Mantin, D.; Cravatt, B. F.; Rayo, J.; Meijler, M. M. Proteome-Wide Mapping of PQS-Interacting Proteins in *Pseudomonas Aeruginosa*. *Chem. Sci.* **2018**, *9* (8), 2290–2294.
(35) Fridman, M.; Solomon, D.; Yogev, S.; Baasov, T. One-Pot Synthesis of Glucosamine Oligosaccharides. *Org. Lett.* **2002**, *4* (2), 281–283.
(36) Adinolfi, M.; Barone, G.; Napoli, L. D.; Guariniello, L.; Iadonisi, A.; Piccialli, G. Solid Phase Glycosidation of Oligonucleotides. *Tetrahedron Lett.* **1999**, *40* (13), 2607–2610.
(37) Melean, L. G.; Love, K. R.; Seeberger, P. H. Toward the Automated Solid-Phase Synthesis of Oligoglucosamines: Systematic Evaluation of Glycosyl Phosphate and Glycosyl Trichloroacetimidate Building Blocks. *Carbohydr. Res.* **2002**, *337* (21–23), 1893–1916.
(38) Gening, M. L.; Tsvetkov, Y. E.; Pier, G. B.; Nifantiev, N. E. Synthesis of β-(1→6)-Linked Glucosamine Oligosaccharides Corresponding to Fragments of the Bacterial Surface Polysaccharide Poly-N-Acetylglucosamine. *Carbohydr. Res.* **2007**, *342* (3–4), 567–575.
(39) Little, D. J.; Poloczek, J.; Whitney, J. C.; Robinson, H.; Nitz, M.; Howell, P. L. The Structure- and Metal-Dependent Activity of *Escherichia Coli* PgaB Provides Insight into the Partial De- *N* -Acetylation of Poly-β-1,6- *N* -Acetyl-d-Glucosamine. *J. Biol. Chem.* **2012**, *287* (37), 31126–31137.
(40) Maira-Litran, T.; Kropec, A.; Goldmann, D. A.; Pier, G. B. Comparative Opsonic and Protective Activities of Staphylococcus Aureus Conjugate Vaccines Containing Native or Deacetylated Staphylococcal Poly-N-Acetyl- -(1-6)-Glucosamine. *Infect. Immun.* **2005**, *73* (10), 6752–6762.
(41) Dasgupta, S.; Nitz, M. Use of *N* , *O* -Dimethylhydroxylamine As an Anomeric Protecting Group in Carbohydrate Synthesis. *J. Org. Chem.* **2011**, *76* (6), 1918–1921.
(42) Dang, C.-H.; Nguyen, C.-H.; Nguyen, T.-D.; Im, C. Synthesis and Characterization of N-Acyl-Tetra-O-Acyl Glucosamine Derivatives. *RSC Adv.* **2014**, *4* (12), 6239.
(43) Yudina, O. N.; Gening, M. L.; Tsvetkov, Y. E.; Grachev, A. A.; Pier, G. B.; Nifantiev, N. E. Synthesis of Five Nona-β-(1→6)-d-Glucosamines with

Various Patterns of N-Acetylation Corresponding to the Fragments of Exopolysaccharide of Staphylococcus Aureus. *Carbohydr. Res.* **2011**, *346* (7), 905–913.

(44) Winkler, A.; Dominguez-Nuñez, J.; Aranaz, I.; Poza-Carrión, C.; Ramonell, K.; Somerville, S.; Berrocal-Lobo, M. Short-Chain Chitin Oligomers: Promoters of Plant Growth. *Mar. Drugs* **2017**, *15* (2), 40.

(45) Ibrahim, K.; El-Eswed, B.; Abu-Sbeih, K.; Arafat, T.; Al Omari, M.; Darras, F.; Badwan, A. Preparation of Chito-Oligomers by Hydrolysis of Chitosan in the Presence of Zeolite as Adsorbent. *Mar. Drugs* **2016**, *14* (8), 43.

(46) Trombotto, S.; Ladavière, C.; Delolme, F.; Domard, A. Chemical Preparation and Structural Characterization of a Homogeneous Series of Chitin/Chitosan Oligomers. *Biomacromolecules* **2008**, *9* (7), 1731–1738.

(47) Chan, P.; Kurisawa, M.; Chung, J. E.; Yang, Y.-Y. Synthesis and Characterization of Chitosan-g-Poly(Ethylene Glycol)-Folate as a Non-Viral Carrier for Tumor-Targeted Gene Delivery. *Biomaterials* **2007**, *28* (3), 540–549.

(48) Kleiner, P.; Heydenreuter, W.; Stahl, M.; Korotkov, V. S.; Sieber, S. A. A Whole Proteome Inventory of Background Photocrosslinker Binding. *Angew. Chem. Int. Ed.* **2017**, *56* (5), 1396–1401.

(49) Hayakawa, K.; Yodo, M.; Ohsuki, S.; Kanematsu, K. Novel Bicycloannulation via Tandem Vinylation and Intramolecular Diels-Alder Reaction of Five-Membered Heterocycles: A New Approach to Construction of Psoralen and Azapsoralen. *J. Am. Chem. Soc.* **1984**, *106* (22), 6735–6740.

(50) Walko, M.; Hewitt, E.; Radford, S. E.; Wilson, A. J. Design and Synthesis of Cysteine-Specific Labels for Photo-Crosslinking Studies. *RSC Adv.* **2019**, *9* (14), 7610–7614.

(51) Qiu, Y.; Li, D. Bifunctional Inhibitors of Mevalonate Kinase and Mevalonate 5-Diphosphate Decarboxylase. *Org. Lett.* **2006**, *8* (6), 1013–1016.

(52) Bohorov, O.; Andersson-Sand, H.; Hoffmann, J.; Blixt, O. Arraying Glycomics: A Novel Bi-Functional Spacer for One-Step Microscale Derivatization of Free Reducing Glycans. *Glycobiology* **2006**, *16* (12), 21C-27C.

(53) Prudden, A. R.; Chinoy, Z. S.; Wolfert, M. A.; Boons, G.-J. A Multifunctional Anomeric Linker for the Chemoenzymatic Synthesis of Complex Oligosaccharides. *Chem Commun* **2014**, *50* (54), 7132–7135.

(54) Østergaard, M.; Christensen, N. J.; Hjuler, C. T.; Jensen, K. J.; Thygesen, M. B. Glycoconjugate Oxime Formation Catalyzed at Neutral PH: Mechanistic Insights and Applications of 1,4-Diaminobenzene as a Superior Catalyst for Complex Carbohydrates. *Bioconjug. Chem.* **2018**, *29* (4), 1219–1230.